Purification, Characterization, and Synthesis of Three Novel Toxins from the Chinese Scorpion *Buthus martensi*, Which Act on K^+ Channels

Régine Romi-Lebrun,*,‡ Bruno Lebrun,‡ Marie-France Martin-Eauclaire,§ Masaji Ishiguro,‡ Pierre Escoubas,‡ Fang Qi Wu,|| Miki Hisada,‡ Olaf Pongs,⊥ and Terumi Nakajima‡

Suntory Institute for Bioorganic Research, Mishima-Gun, Shimamoto-Cho, Wakayamadai 1-1-1, Osaka 618, Japan, Centre National de la Recherche Scientifique, UMR 6560, Laboratoire de Biochimie, Faculté de Médecine Nord, 13916 Marseille Cedex 20, France, Sichuan Province Institute for Antibiotics, Sanbanqiao 9, Chengdu, China, and Zentrum für Molekulare Neurobiologie, Institut für Neurale Signalverarbeitung, Martinistrasse 52, Haus 42, D-20246 Hamburg, Germany

Received May 5, 1997; Revised Manuscript Received August 19, 1997⊗

ABSTRACT: Three novel toxins belonging to the scorpion K^+ channel-inhibitor family were purified to homogeneity from the venom of the Chinese scorpion *Buthus martensi*. They have been identified according to their molecular mass (3800−4300 Da) and their neurotoxicity in mice and characterized as 37-amino acid peptides. One of them shows 81−87% sequence identity with members of the kaliotoxin group (named BmKTX), whereas the other two, named BmTX1 and BmTX2, show 65−70% identity with toxins of the charybdotoxin group. Their chemical synthesis by the Fmoc methodology allowed us to show that BmKTX, unlike BmTX1 and BmTX2, possesses an amidated C-terminal extremity. Toxicity assays *in vivo* established that they are lethal neurotoxic agents in mice (LD_{50}s of 40−95 ng per mouse). Those toxins proved to be potent inhibitors of the voltage-gated K^+ channels, as they were able to compete with [^{125}I]kaliotoxin for its binding to rat brain synaptosomes (IC_{50}s of 0.05−1 nM) and to block the cloned voltage-gated K^+ channel Kv1.3 from rat brain, expressed in *Xenopus* oocytes (IC_{50}s of 0.6−1.6 nM). BmTX1 and BmTX2 were also shown to compete with [^{125}I]charybdotoxin for its binding to the high-conductance Ca^{2+}-activated K^+ channels present on bovine aorta sarcolemmal membranes (IC_{50}s of 0.3−0.6 nM). These new sequences show multipoint mutations when compared to the other related scorpion K^+ channel toxins and should prove to be useful probes for studying the diverse family of K^+ channels.

Scorpion venoms contain several dozen toxins which have proven to be high-affinity ligands of ion channels and therefore constitute useful pharmacological probes for their study (*1*, *2*). Two main groups of toxins have been distinguished according to their pharmacological properties; they either modulate the activity of Na^+ channels from excitable cells (the major group) or specifically block K^+ channels (*3*). This pharmacological classification also matches the structural properties of this peptide family, since toxins directed against Na^+ channels are composed of a polypeptidic chain of 60−80 amino acids reticulated by four disulfide bridges, versus 30−40 amino acids and three or four disulfide bridges for those active on K^+ channels.

Toxins acting on K^+ channels have been identified more recently, and formal classification has been rendered difficult by the lack of high selectivity of those toxins toward the various subtypes of K^+ channels. Those toxins act on Ca^{2+}-activated K^+ channels [small (SK_{Ca})[1] or large (BK_{Ca}) conductance] and/or on various voltage-gated K^+ channels (K_v) (*2*). Although one small group of toxins was shown to include selective blockers of the SK_{Ca} channels (*4*−*6*), the other toxins act in a large affinity range on several subtypes of voltage-gated K^+ channels as well as on the BK_{Ca} channels. On the basis of amino acid sequences, those latter toxins can be classified into four distinct groups with 50−80% sequence identity within a group, and less than 50% between members of different groups (*7*−*10*). This classification is not exhaustive as several toxins have been recently isolated. The first group contains charybdotoxin (ChTX) and Lq2 from *Leiurus quinquestriatus hebraeus* (*11*, *12*) and iberiotoxin (IbTX) from *Buthus tamulus* (*13*). The second group includes the kaliotoxins (KTX) from *Androctonus* scorpions (*14*, *15*) and the agitoxins (AgTX) from *L. quinquestriatus hebraeus* (*7*), with 80−90% sequence identity. Noxiustoxin (NTX) from *Centruroides noxius* (*16*), margatoxin (MgTX) from *Centruroides margaritatus* (*17*), and TsKα from *Tityus serrulatus* (*18*) define the third group with 60−80% sequence identity with each other. Only very recently, a fourth group emerged which encompasses toxins with 35 amino acid residues and three or four disulfide bridges, all isolated from scorpions belonging to the Scorpionidae family, *Pandinus imperator* [Pi1, Pi2, and Pi3 (*9*, *10*)], and *Scorpio maurus* [maurotoxin (MTX) (*19*)]. They display 50−70% sequence identity with each other, and less than 50% sequence identity with the other toxins.

All scorpion K^+ channel inhibitors have been shown to possess a similar three-dimensional structure, characterized

* To whom correspondence should be addressed.
‡ Suntory Institute for Bioorganic Research.
§ UMR 6560.
|| Sichuan Province Institute for Antibiotics.
⊥ Institut für Neurale Signalverarbeitung.
⊗ Abstract published in *Advance ACS Abstracts*, October 1, 1997.
[1] Abbreviations: ChTX, charybdotoxin; IbTX, iberiotoxin; KTX, kaliotoxin; AgTX, agitoxin; NTX, noxiustoxin; MgTX, margatoxin; MTX, maurotoxin; SK_{Ca}, small conductance Ca^{2+}-activated K^+ channels; BK_{Ca}, big conductance Ca^{2+}-activated K^+ channels; K_v, voltage-gated K^+ channels; MALDI-TOF, matrix-assisted laser desorption/ionization time-of-flight; HPLC, high-pressure liquid chromatography; CZE, capillary zone electrophoresis; LD_{50}, 50% lethal dose; icv, intracerebroventricular.

S0006-2960(97)01044-1 CCC: $14.00

by an α-helix and a β-sheet, stabilized by disulfide bridges (*20*). Many groups have extensively studied the structural elements crucial for the activity of some of the toxins, by monopoint mutational experiments [ChTX (*21*, *22*)] or by chemical synthesis of small peptides [KTX (*23*, *24*)] and chimera [ChTX/IbTX (*25*)]. To extend such studies, new analogues are required, and new natural ones may offer the advantage of being active structures with multipoint mutations compared to already known toxins.

We have investigated the venom of the Chinese scorpion *Buthus martensi* for its content in toxins active on K^+ channels. This venom has been poorly characterized so far, since it is hardly available outside of China. Only a few neurotoxins selective of the insect and mammalian Na^+ channels have been previously described (*26*, *27*). We have recently reported the purification and characterization of four peptides with molecular masses (M_r) of 2900−3200 Da from *B. martensi*, which are active on the apamin-sensitive SK_{Ca} channels (*6*). In this paper, we report the physicochemical characterization of three new toxins from the same scorpion venom, with molecular masses (M_r) of 3900−4300 Da, showing high sequence homology with the other scorpion toxins [preliminary results were reported in an abstract form (*28*)]. We describe their pharmacological properties (i) toward the K_v channels, in competition assays against [^{125}I]-KTX on rat brain synaptosomes and in electrophysiological experiments using the rat brain Kv1.3 channel [also called RCK3 (*29*)] expressed in *Xenopus* oocytes; and (ii) toward the BK_{Ca} channels, in competition assays against [^{125}I]ChTX on bovine aorta sarcolemmal membranes. These toxins have been identified by a nonconventional approach using their molecular mass, determined by matrix-assisted laser desorption/ionization time-of-flight mass spectrometry (MALDI-TOF-MS) analysis of the fractionated crude venom, and their toxicological properties in mice. Due to their low representation in *B. martensi* venom (below 0.05% w/w), these peptides were chemically synthesized in the solid phase and the synthetic molecules were used for further characterization of the biological properties. They are highly toxic toward mice and were shown to interact at low concentrations (less than 1 nM) with the voltage-gated K^+ channels which are targeted by KTX, on rat brain synaptosomes. They also block the rat Kv1.3 channel expressed in *Xenopus* oocytes with IC_{50}s in the nanomolar range. Kv1.3 channel has been found in several types of cells, in neurons, and in T-lymphocytes and has proven to be highly sensitive to scorpion toxins (*30*). At a nanomolar range affinity, two among those toxins also competed with [^{125}I]ChTX for interaction with its receptor site which is associated with the BK_{Ca} channels on bovine smooth muscle. Structure−activity relationships of these new K^+ channel toxins are discussed in this paper.

EXPERIMENTAL PROCEDURES

Purification of the Toxins. B. martensi scorpion venom was obtained by manual or electric stimulation of the postabdomen of scorpions bred in captivity in Chengdu (China). Lyophilized venom (300 mg) was prepared as previously described (*6*).

The soluble venom, extracted with acetic acid, was loaded in batches of about 60 mg onto a C18 reversed-phase semipreparative HPLC column (see details in the legend of Figure 1). Fractions 4, 6, and 7 containing the three peptides were collected, lyophilized, and subsequently purified by cation-exchange HPLC (conditions are given in the legend of Figure 2). A desalting step on C18 reversed-phase HPLC allowed us to obtain homogeneous toxins. The C18 column (Merck, 12.5 × 0.4 cm, 100 Å, 5 μm bead size) was equilibrated in 0.1% trifluoroacetic acid in water, and a linear gradient of solvent B (0.1% trifluoroacetic acid in acetonitrile) in solvent A (0.1% trifluoroacetic acid in water) was applied from 5 to 40% over 20 min (BmKTX), from 0 to 40% over 40 min (BmTX1), and from 0 to 40% over 20 min (BmTX2).

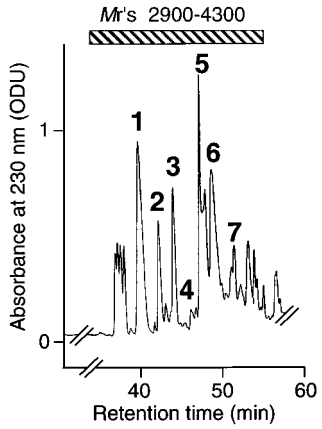

FIGURE 1: Part of the reversed-phase C18 HPLC profile of the soluble venom from the *B. martensi* scorpion. The column (Shiseido Capcell pak, 25 × 1 cm, 120 Å, 5 μm bead size) was equilibrated in 0.1% trifluoroacetic acid in water. A linear gradient of 0.1% trifluoroacetic acid in acetonitrile was applied from 0 to 45% over 102 min at a flow rate of 3 mL/min and an absorbance reading of 230 nm. The fractions which show toxicity toward mice and contain low-molecular mass components (2900−4300 Da) are numbered 1−7. Toxic components with higher molecular masses eluted later (see the complete chromatogram in ref 6).

Physicochemical Characterization. In this report, the toxins previously coded Bm14-VI, Bm16-IX, and Bm17-XI (*28*) have been renamed BmKTX, BmTX1, and BmTX2, respectively.

Amino Acid Composition. The amino acid composition of each purified peptide was determined after acid hydrolysis [6 N HCl/1% (w/v) phenol] under vacuum at 110 °C for 20 h. Amino acid standards (Pierce, Rockford, IL) and dried hydrolyzed samples were derivatized with phenyl isothiocyanate (Wako Chemical Ind. Ltd., Osaka, Japan), as previously described (*6*).

Sequence Determination of BmKTX. Prior to sequence examination, 2 nmol of BmKTX was reduced by tri-*n*-butylphosphine and pyridylethylated *in situ* by 4-vinylpyridine, according to the method described by Ruegg and Rudinger (*31*). The pyridylethylated BmKTX was subsequently desalted by C18 reversed-phase HPLC, and Edman degradation was performed in an automated Shimadzu PPSQ10 gas-phase sequencer, as previously described (*6*).

Sequence Determination of BmTX1 and BmTX2. Three to six nanomoles was reduced by dithiothreitol and S-carboxymethylated with sodium iodoacetate, as previously described (*23*). The N terminus was subsequently unblocked by treatment with pyroglutamate aminopeptidase (Boehringer, Mannheim, Germany), under the experimental conditions used for ChTX (*11*) or IbTX (*13*). Sequencing of N-unblocked peptides was performed as that for BmKTX.

Cleavage of BmTX1 and BmTX2. The S-carboxymethylated peptides were cleaved by CNBr (BmTX1) or by

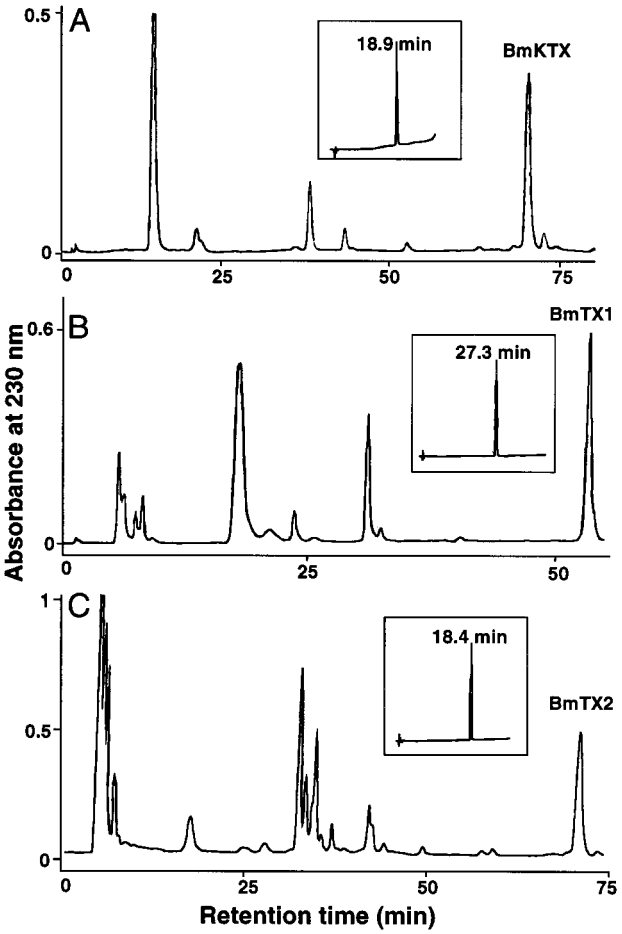

FIGURE 2: Purification of the toxins. BmKTX, BmTX1, and BmTX2 were purified by cation-exchange chromatography of C18 HPLC fraction 4 (chromatogram A), fraction 6 (chromatogram B), and fraction 7 (chromatogram C), respectively, followed by a desalting step on C18 HPLC (insets). Briefly, C18 HPLC fractions 4, 6, and 7, shown in Figure 1, were lyophilized, resolubilized in 10 mM sodium phosphate at pH 6.8, and further fractionated by using a cation-exchange HPLC column (Tosoh, TSK-gel, sulfopropyl SP-5PW, 0.6 × 7 cm), equilibrated in the same buffer. A linear gradient of buffer B, made up of 1 M NaCl (fractions 4 and 6) or 800 mM NaCl (fraction 7) in 10 mM sodium phosphate at pH 6.8, was applied over 80 min at a flow rate of 0.5 mL/min and an absorbance reading of 230 nm. BmKTX, BmTX1, and BmTX2, as indicated in their respective fraction, were eluted by 560, 580, and 600 mM NaCl in 10 mM sodium phosphate at pH 6.8, respectively [chromatograms A−C represent an aliquot of about $^1/_3$, $^1/_{15}$, and $^1/_6$ (v/v) of the total volume of fractions 4, 6, and 7, respectively, collected from the semipreparative C18 HPLC of 300 mg of soluble venom]. Desalting and final purification by reversed-phase C18 HPLC of each toxin are shown in the inset (see Experimental Procedures for the conditions).

lysine-C-endoprotease (*Achromobacter* protease I, Takara, Tokyo, Japan) (BmTX2). Two C-terminal CNBr fragments of BmTX1 were obtained and purified as previously described (*23*), and then sequenced as above. Three fragments mapping the C terminus of BmTX2 were obtained as follows; 3.5 nmol of S-carboxymethylated peptide was cleaved with an enzyme-to-protein ratio of 1:200 (w/w) in 10 mM Tris-HCl at pH 9 and 37 °C for 16 h, and the subsequent peptides were then separated with C18 HPLC, under the same conditions as those for the CNBr fragments of BmTX1, and sequenced (see above).

Capillary Electrophoresis. Capillary electrophoresis analyses were performed on a Jasco CE-800 system, as previously described (*6*). Samples of natural and synthetic BmKTX were dissolved in 20 mM sodium citrate buffer (pH 2.5) and applied hydrodynamically to the capillary, separately or together.

Mass Spectrometry Analysis. The molecular mass of components of a mixture (C18 HPLC fractions), or purified toxins, was determined on a MALDI-TOF mass spectrometer (PerSeptive Voyager Elite). All mass spectra were recorded in the linear mode, except for that of BmKTX which was also measured in the reflector mode. Preparation of samples and analysis of spectra were carried out as previously described (*6*).

Chemical Synthesis. Solid-phase synthesis of BmKTX, BmTX1, and BmTX2 was performed on an Applied Biosystems 433A peptide synthesizer, using the same FastMoc program and reagents as described previously (*6*). All the peptides were assembled stepwise in a small reactor, on 0.1 mmol of resin preloaded with Fmoc-Lys(Boc) (for BmKTX) or Fmoc-Ser(tBu) (for both BmTX1 and BmTX2), at 0.65 mmol of amino groups/g. Side chain protecting groups used for trifunctional residues were as follows: trityl (Trt) for Asn, Cys, Gln, and His; *tert*-butyl ester (OtBu) for Asp and Glu; butyloxycarbonyl (Boc) for Lys; *tert*-butyl for Ser, Thr, and Tyr; and Ng-2,2,5,7,8-pentamethylchroman-6-sulfonyl (Pmc) for Arg. After full assembly, each peptidyl resin was dried and cleaved by the mixture TFA/thioanisol/ethanedithiol, and the resulting peptides were extracted with cold diethyl ether as previously described (*6*). Dried crude peptides were readily dissolved in pure water (1.7 mM), and the six free cysteine residues were allowed to oxidize by air exposure in a basic aqueous triethylamine solution at room temperature for 40 h. Purification to homogeneity of oxidized peptides was carried out on a semipreparative C18 reversed-phase HPLC column, using a gradient of acetonitrile in water, under the same conditions as described previously (*6*). The identity of synthetic and natural products was checked by amino acid analysis after acid hydrolysis, by a C18 HPLC co-injection experiment (BmTX1 and BmTX2), by capillary electrophoresis (BmKTX), and by mass spectrometry analysis. Synthetic toxins are noted sBmKTX, sBmTX1, and sBmTX2.

Toxicity Assay in Mice. Prior to injections, both C18 HPLC fractions from *B. martensi* venom (aliquots corresponding to $^1/_{500}$ of the collected volume per fraction) and purified toxins were lyophilized and then diluted in a solution containing 20 mg/mL BSA and 9 mg/mL NaCl. Intracerebroventricular injections of 5 μL of each sample were performed on 20 g male mice (C57Bl/6). The 50% lethal dose (LD_{50}) of the purified synthetic peptides was calculated according to the formula of Behrens and Karber (*32*), using a range of doses as previously described (*23*).

Competition Binding Assays on Rat Brain Synaptosomes. Rat brain synaptic nerve-ending particles (synaptosomes, P2 fraction) were prepared according to Gray and Whittaker (*33*). The protein content was assayed by a modified Lowry method. Kaliotoxin (KTX) was radiolabeled using the iodogen method as described previously (*15*, *23*). The specific radioactivity of 2000 Ci/mmol was routinely obtained for the monoiodo derivative. Competition assays were performed as described previously (*15*, *23*). Nonspecific binding was determined in the presence of an excess (0.1 μM) of unlabeled kaliotoxin and was less than 25% of the total binding. Data points correspond to three independent experiments performed in duplicate. IC_{50}s were determined

by least-squares fitting of the equation $B/B_0 = 1 +$ [unlabeled toxin]/IC_{50} to data points.

Competition Binding Assays on Bovine Aortic Sarcolemmal Membranes. Highly purified sarcolemmal membranes were prepared as previously described (*34*). Competition experiments using [^{125}I]ChTX (2000 Ci/mmol), purchased at NEN-Dupont (Wilmington, DE), were performed in triplicate or quadruplicate as previously described (*35*). Briefly, sarcolemmal membranes vesicles (6 μg) were incubated with 140 pM [^{125}I]ChTX in 20 mM NaCl, 20 mM Tris-HCl (pH 7.4), 0.1% BSA, and 0.1% digitonin in the absence or presence of increasing concentrations of unlabeled ChTX, or the Bm toxins. Incubations were carried out at room temperature until equilibrium was achieved. At the end of the incubation period (1 h), samples were diluted with 4 mL of ice-cold 100 mM NaCl and 20 mM Hepes/Tris (pH 7.4), rapidly filtered through GF/C filters that had been presoaked in 0.3% poly(ethyleneimine), and washed two times with ice-cold medium. Nonspecific binding was evaluated with an excess of unlabeled ChTX (10−100 nM). Under these conditions, nonspecific binding represents less than 3% of the total radioactivity added. Data points are the mean of triplicate or quadruplicate assays performed in two to five independent experiments. IC_{50}s were determined as described above.

Kv1.3 Channel Expression. The rat Kv1.3 channel gene was inserted into a pAS18 vector. The plasmid was linearized with *Eco*RI, and the clone was transcribed *in vitro* with SP6 RNA polymerase, using a transcription kit (Stratagene Inc., La Jolla, CA). cRNA was injected into *Xenopus laevis* oocytes 16−72 h prior to electrophysiological recordings.

Electrophysiological Recordings. Oocytes were impaled by two microelectrodes filled with 3 M KCl (resistance of 0.5−2 MΩ) and voltage-clamped using an Axoclamp-2B two-electrode voltage clamp amplifier in the bath-clamp mode interfaced to a personal computer running the Pclamp 6.0 software, with a Digidata analog/digital board (Axon Instruments, Inc., Foster City, CA). Currents were low-pass filtered at 1 kHz with an eight-pole Bessel filter (CyberAmp 320, Axon Instruments) and digitized at 10 kHz. The holding potential was −80 mV with less than −40 nA of holding current. Pulses were delivered at a rate of one every 60 s, to allow full recovery from inactivation. Capacitive and leak currents were subtracted on-line, using a P/2 protocol. Oocytes were bathed in an ND96 solution [0.3 mM $CaCl_2$, 1 mM $MgCl_2$, 2 mM KCl, 96 mM NaCl, and 5 mM Hepes (pH 7.6) with NaOH] supplemented with 50 mg/L BSA. The 100 μL recording chamber was perfused with ND96 flowing from one of several reservoirs, at a flow of 4 mL/min. Switching from one reservoir to another was carried out with Isolatch Teflon valves (General Valves Corp., Fairfield, NJ). All measurements were made at room temperature (∼22 °C). IC_{50}s were determined by least-squares fitting of the equation $I_X = 1/(1+ X/IC_{50})$ to data points (I_X is the normalized K^+ current amplitude measured during the perfusion of the toxin at concentration X).

Modeling of BmKTX and BmTX2. A preliminary structure model of BmKTX was generated by substituting residues of a three-dimensional structure of agitoxin 2 (AgTX2), which is available from the Brookhaven Protein Data Bank (accession number 1AGT). This structure was then energy-optimized in a water bath generated in the 5 Å around the peptide, using Discover-3 (Molecular Simulations Inc.) on an Indigo 2 workstation, until rms derivatives became less than 10^{-3} kcal mol^{-1} Å^{-1}. The structure-optimized BmTX2 was also obtained in the same way using the charybdotoxin structure deposited in the Brookhaven Protein Data Bank (1CHL).

RESULTS

Purification and Physicochemical Characterization of B. martensi Toxins. Toxins with small molecular masses (2900−4300 Da) have been identified by screening the peptide-containing C18 HPLC fractions of *B. martensi* crude venom for their toxicological activity and mass range of their constituents (Figure 1, HPLC profile showing the area of fractions 1−7; for the other fractions, see the complete profile in ref 6). These toxins were eluted early on reversed-phase C18 HPLC, by the lowest concentration in acetonitrile, when compared with toxins with larger molecular masses (6000−8000 Da) (not shown). The knowledge of the molecular mass of scorpion toxins may serve as a useful indicator of the pharmacological type of toxins. Scorpion toxins which block K^+ channels have a mass in the range 3000−4000 Da, whereas those acting on Na^+ channels have larger molecular masses (6000−8000 Da). Fractions 1−3 and 5 were shown to contain peptides with molecular masses (M_r) of 2900−3200 Da, displaying high sequence similarities with the P01−P05 and leiurotoxin peptides, and able to bind to the apamin-sensitive Ca^{2+}-activated K^+ channels (*6*). Aliquots of fractions 4, 6, and 7 induced highly toxic symptoms by icv injection in mice, which died in convulsions, within a 0.5−2 h time interval. These fractions were further purified by cation-exchange HPLC (Figure 2), and each peak was assayed again for its toxicity in mice. One highly active peptide, lethal to mice, was identified in each of those fractions. They were the last peptides to elute from the cation-exchange column with a high concentration of sodium chloride (about 0.6 M) (Figure 2), which indicated their highly basic character. The three active peptides, named BmKTX, BmTX1, and BmTX2, were further purified to homogeneity by reversed-phase C18 HPLC (insets in Figure 2) and then subjected to chemical analysis. Their representation in the venom was assessed by the ratio of the quantity of peptides, determined by amino acid analysis, to the initial quantity of crude venom treated (300 mg); BmKTX, BmTX1, and BmTX2 amounted to 0.020, 0.033, and 0.027% of the venom, respectively. Amino acid compositions obtained on native peptides after acid hydrolysis are shown in Table 1. The presence of six cysteine residues was hypothesized to match the calculated and experimental molecular masses. Sequencing of BmKTX was performed with overall repetitive and initial yields of 91.8 and 83%, respectively. The sequence was in accordance with both the amino acid composition and the experimental molecular mass (BmKTX, Figure 3). Conversely, the experimental masses of BmTX1 and BmTX2 were 16−18 Da lower than those deduced from the amino acid composition (see the bottom of Table 1). This discrepancy could be explained by the loss of water (18 Da) of a glutamic acid residue located in an N-terminal position, resulting in a pyroglutamic acid. This hypothesis was confirmed by the failure of a first attempt at sequencing of the reduced and pyridylethylated derivatives of BmTX1 and BmTX2, in agreement with a blocked N-terminal extremity. The amino terminus of these peptides was therefore un-

Table 1: Amino Acid Compositions

amino acids	BmKTX	BmTX1	BmTX2
Asx	3.7 (4)	2.7 (3)	1.9 (2)
Glx	1.0 (1)	2.9 (3)	2.1 (2)
Ser	1.0 (1)	2.0 (2)	5.6 (6)
Gly	5.0 (5)	4.2 (4)	2.2 (2)
His	1.0 (1)	−	−
Thr	1.0 (1)	2.0 (2)	2.0 (2)
Ala	1.1 (1)	−	1.1 (1)
Pro	2.0 (2)	2.2 (2)	1.0 (1)
Arg	1.0 (1)	1.1 (1)	2.0 (2)
Tyr	−	0.9 (1)	1.8 (2)
Val	1.9 (2)	2.0 (2)	2.0 (2)
Met	1.0 (1)	2.0 (2)	1.0 (1)
Cys	1.3[a]	1.0[a]	1.3[a]
Ile	1.9 (2)	−	−
Leu	1.1 (1)	−	1.2 (1)
Phe	0.9 (1)	1.9 (2)	1.9 (2)
Lys	6.6 (7)	5.6 (6)	3.7 (4)
absorance[b] at 280 nm	−	+ (1Trp)	+ (1Trp)
calcd M_r (Da)	3962.8	4185.8	4198.7
expt M_r (Da)	3961.3	4169.1	4182.2

[a] Cys residues were partially decomposed after acid hydrolysis. [b] The spectrum of Trp residues was analytically recorded on a diode array detector, during C18 HPLC of the purified BmTX1 and BmTX2 (not shown). Experimental masses were determined by MALDI-TOF-MS.

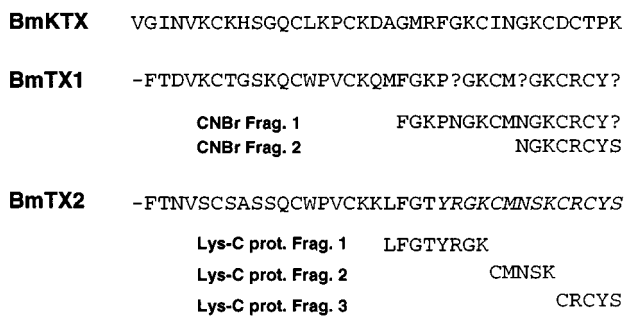

FIGURE 3: Amino acid sequence determination. The sequence of BmKTX was completely determined on the reduced and pyridylethylated peptide (see Experimental Procedures for the conditions). Reduced and S-carboxymethylated BmTX1 and BmTX2 were first treated by pyroglutaminase, to remove the pyroglutamic acid residue blocking the N-terminal part of the peptides (represented by a dash). The C-terminal sequence of BmTX1 was achieved after sequencing two fragments obtained by CNBr cleavage at both methionine residues. The C-terminal sequence of BmTX2 was unambiguously deduced after cleavage by lysine-C-protease and sequencing of three C-terminal fragments.

blocked by treatment with a pyroglutamic acid aminopeptidase, and then sequencing could be carried out for almost 36 cycles. Sequencing of BmTX1 displayed an overall repetitive yield of 94.4% until the 24th step, where a drastic decrease to 78.6% was observed, followed by a second drop at the 29th step. As the PTH amino acids could not be attributed unambiguously for these two steps, further sequencing of the C-terminal part was necessary; two overlapping fragments obtained by CNBr cleavage allowed us to determine the presence of one Asn, at both positions (BmTX1, Figure 3). Moreover, this experiment allowed the identification of one serine residue at the C-terminal end of the toxin, which had escaped the first analysis. One explanation which could be proposed to explain the decrease in the yield of sequencing of the parent molecule is the fact that an Asn−Gly bond is observed at both positions and can be converted into an imide linkage, which is known to be resistant to the Edman degradation (*36*). Similar low yields in sequencing due to this doublet of amino acids had already been mentioned in the structural study of some long toxins from *Androctonus* scorpion venom (*37*). The BmTX2 sequence was obtained in one run, with an overall repetitive yield of 89.6%, but due to very small amounts of PTH amino acids detected for the last 16 steps, examination of the C-terminal part of the molecule was undertaken by sequencing three Lys-C protease fragments (BmTX2, Figure 3). All those toxins are composed of a single chain of 37 amino acids, including six cysteine residues, probably connected by three disulfide bonds. At this stage, no data about the nature of the C-terminal extremity of the *B. martensi* toxins were available, the precision of the mass obtained by MALDI-TOF-MS in the linear mode not being reliable enough to discriminate accurately for a 1 mass unit difference which is the mass difference between the $CONH_2$ and COOH groups .

Solid-Phase Synthesis of BmKTX, BmTX1, and BmTX2. To confirm the sequence, to elucidate the C-terminal extremity of each toxin, and to further characterize their biological properties, the chemical synthesis of BmKTX, BmTX1, and BmTX2 was undertaken using optimized Fmoc/*tert*-butyl chemistry, on preloaded resins, to give carboxylic end peptides (*6*). The overall assembly yield was in the range of 83−98%. After acidolytic cleavage with average yields of 60−90%, the crude peptides were then oxidized by exposure to air, at basic pH; as one example, see the analytical HPLC profile of crude synthetic BmKTX (named sBmKTX) in trace 1 of Figure 4A. Those of the other peptides are not shown as they all displayed similar chromatographic behavior. All peptides were correctly oxidized as a peak corresponding to an active peptide appeared during the course of oxidation (see trace 2 of Figure 4A, sBmKTX, t = 16.83 min), at the same time as the disappearance of the reduced form at t = 19.98 min. The synthetic oxidized forms of BmKTX, BmTX1, and BmTX2 were shown to be neurotoxic to mice and were further purified to homogeneity by semipreparative HPLC (see the analytical HPLC of sBmKTX in trace 3 of Figure 4A). The yield of oxidation estimated by the ratio of oxidized homogeneous peptide, determined by amino acid analysis, to the initial amount of crude peptide was 11.4% (BmKTX), 6% (BmTX1), and 8% (BmTX2). Mass data for sBmTX1 and sBmTX2 were in agreement with those of the natural ones, including a pyroglutamic acid in the N-terminal position (synthetic BmTX1, M_r = 4170.6 Da; natural BmTX1, M_r = 4169.1 Da; synthetic BmTX2, M_r = 4181.4 Da; and natural BmTX2, M_r = 4182.1 Da). Each of those synthetic peptides gave the same amino acid composition as those of their natural homologues (not shown). sBmTX1 and sBmTX2 also eluted in a single sharp peak by C18 HPLC, when co-injected with their natural form (not shown). However, sBmKTX was the only peptide which showed results not in agreement with the structural features of its natural homologue, as both forms did not coelute, neither by C18 HPLC (not shown) nor by CZE (see Figure 4B; the natural peptide eluted later, which indicated a character more basic than the synthetic one). Moreover, the mass data obtained in the reflector mode on MALDI-TOF-MS gave a mass lower by 1 unit for the natural BmKTX when compared to the synthetic one (traces 1 and 2 of Figure 4C), in accordance with an amidated form (theoretical monoisotopic

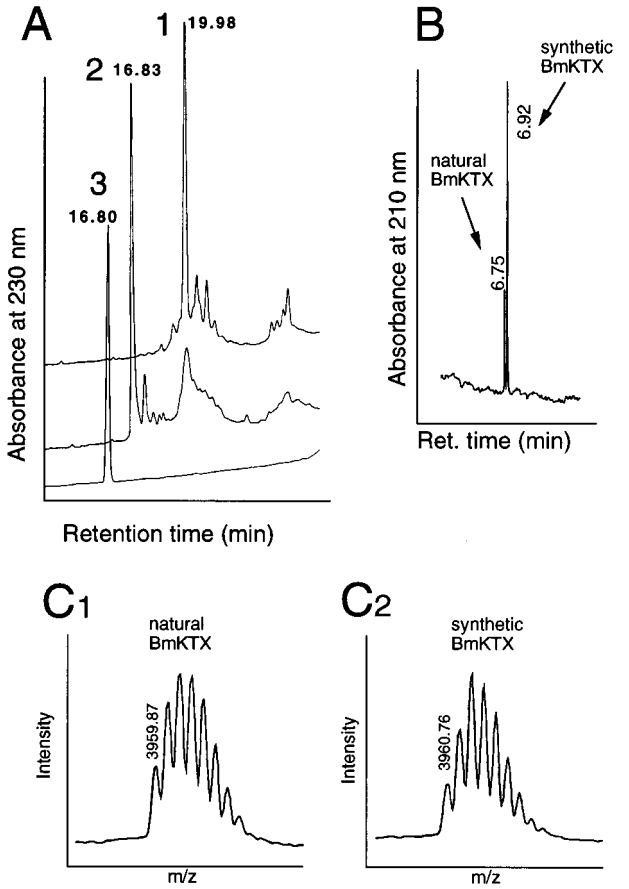

FIGURE 4: Comparison of natural and synthetic BmKTX. (A) Analytical reversed-phase C18 HPLC profiles of crude reduced sBmKTX after TFA cleavage (1) (crude sBmKTX) and after 40 h of oxidation (2) and purified oxidized sBmKTX (3). The HPLC conditions are the same as those in the inset of Figure 2C. (B) Capillary electrophoresis of co-injected natural and synthetic BmKTX. A 2-fold molar excess of synthetic toxin to the natural one was injected. Separate injections showed that the natural BmKTX eluted at $t = 6.74$ min and the synthetic toxin at $t = 6.92$ min (not shown). Details of the conditions are described in Experimental Procedures. (C) MALDI-TOF mass spectra of natural (C_1) and synthetic BmKTX (C_2) obtained in the reflector mode. Ions [$(M + H)^+$] are indicated, corresponding to a monoisotopic mass of 3958.87 Da for the natural BmKTX, 1 mass unit lower than that of the synthetic one (monoisotopic mass of 3959.76 Da, C_2). We conclude that BmKTX has an amidated C terminus, when compared to its synthetic carboxylated form.

M_r = 3958.88). All these data support an amidated C-terminal end of BmKTX.

Toxicity in Mice. The toxic activity in mice by icv injection was one of the guidelines for identifying those peptides. LD_{50}s were not determined for natural compounds because of a paucity of material but were roughly estimated to be ca. 50 ng per mouse, for BmKTX, BmTX1, and BmTX2. LD_{50}s were therefore assessed on synthetic peptides: sBmKTX, 95.1 ng; sBmTX1, 62.5 ng; and sBmTX2, 53.4 ng. The symptoms observed after injection of doses near the LD_{50}s of either natural or synthetic toxins showed neurotoxicity with hyperexcitability effects, followed by death of the mice within 1 h. However, from the results of these tests, there was a slight difference between the LD_{50} of sBmKTX and the value expected from the natural molecule. To clarify this point, we again purified BmKTX from a new batch of venom, using the same conditions as previously described. Finally, we could determine the LD_{50} of the natural peptide (40.3 ng).

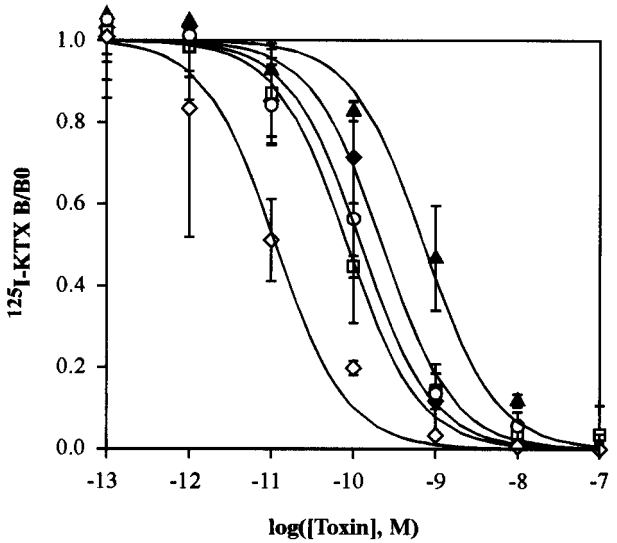

FIGURE 5: Effects of the toxins on [^{125}I]KTX binding to rat brain synaptosomes. Samples of 20 μL of [^{125}I]KTX (40 pM) and 20 μL of increasing concentrations of unlabeled KTX (open diamonds), natural BmKTX (filled diamonds), sBmKTX (filled triangles), sBmTX1 (open squares), or sBmTX2 (open circles) were incubated with 160 μL of synaptosomes suspension (30 μg of protein/assay) in 25 mM Tris-HCl, 50 mM NaCl, and 0.1% (w/v) BSA at pH 7.4 for 1 h at 25 °C. IC_{50} of KTX is 11 ± 3 pM.

Effects of Bm Toxins on Voltage-Gated K^+ Channels. The interaction of Bm toxins with K_v channels was investigated using ligand binding and electrophysiological techniques. In binding experiments, we measured the ability of Bm toxins to affect [^{125}I]KTX binding to the K_v channels present on rat brain synaptosomes. This membrane preparation was shown to contain various K_v channels, constituted by heterotetramers of subunits of Kv1 (*29*, *38*, *39*). Iodinated KTX was shown previously to bind to the dendrotoxin-sensitive K_v channels, on the same preparation (*23*). BmKTX (synthetic and natural), sBmTX1, and sBmTX2 were able to compete with [^{125}I]KTX for binding to its receptor site, with IC_{50}s of 0.2 ± 0.07 nM for natural BmKTX, 0.7 ± 0.3 nM for sBmKTX, 0.09 ± 0.01 nM for sBmTX1, and 0.12 ± 0.03 nM for sBmTX2 (Figure 5).

In electrophysiological experiments, the Bm toxins were tested for their ability to block the cloned voltage-gated rat brain Kv1.3 channel expressed in *Xenopus* oocytes. Natural and synthetic BmKTX, sBmTX1, and sBmTX2 were able to inhibit the rat Kv1.3 current in a concentration-dependent manner (see the K^+ currents blocked by sBmTX2 in Figure 6A), with IC_{50}s of 0.2 ± 0.01, 0.6 ± 0.15, 1.5 ± 0.06, and 1.6 ± 0.13 nM, respectively (see the dose−response curves in Figure 6B).

Effects of Bm Toxins on BK_{Ca} Channels. Figure 7 demonstrates the ability of sBmTX1 and sBmTX2 to compete with [^{125}I]ChTX for binding to the BK_{Ca} channels present on bovine aortic sarcolemmal vesicles. Unlabeled ChTX inhibited [^{125}I]ChTX binding completely with an IC_{50} of 7.2 ± 0.7 pM, a value in agreement with those previously determined in smooth muscle binding experiments for natural ChTX [20 pM (*35*)] or synthetic ChTX [10 pM (*25*)]. sBmTX1 and sBmTX2 were able to compete with [^{125}I]-ChTX on digitonin-treated aortic sarcolemmal vesicles and displayed IC_{50}s of 0.65 ± 0.1 and 0.3 ± 0.06 nM, respectively, unlike sBmKTX which did not show any significant inhibitory activity at concentrations of up to 100 nM.

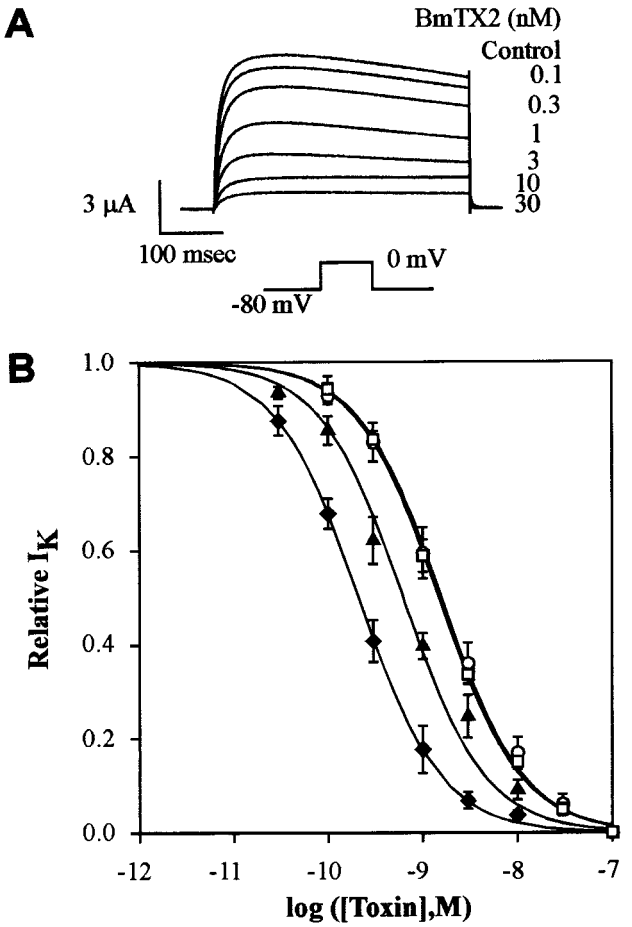

FIGURE 6: BmKTX, BmTX1, and BmTX2 are high-affinity inhibitors of rat Kv1.3 channels. Oocytes expressing rat Kv1.3 channels were recorded under two-electrode voltage clamp. Potassium currents were obtained by depolarization from a holding potential of −80 to 0 mV. Capacitive and leak currents were subtracted on-line using a P/2 protocol. **(**A) Superfusion with the synthetic BmTX2 at the indicated concentrations caused a dose-dependent reversible inhibition of K^+ currents. (B) Dose-dependent inhibition curves of rat Kv1.3 currents by the natural BmKTX (filled diamonds) and the synthetic toxins, sBmKTX (filled triangles), sBmTX1 (open squares), and sBmTX2 (open circles). Data points are the means ± SD of at least four independent experiments. The solid lines through the data are according to the equation $I_X = 1/(1+X/IC_{50})$, with IC_{50}s of 0.2 nM (natural BmKTX), 0.6 nM (sBmKTX), 1.5 nM (sBmTX1), and 1.6 nM (sBmTX2).

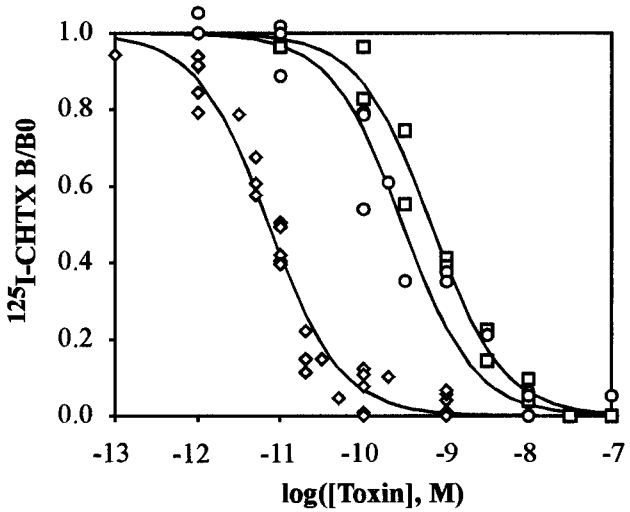

FIGURE 7: Effects of the toxins on [^{125}I]ChTX binding to aortic sarcolemmal membrane vesicles. Sarcolemmal membranes vesicles (6 μg) were incubated with 140 pM [^{125}I]ChTX in 20 mM NaCl, 20 mM Tris-HCl (pH 7.4), 0.1% BSA (w/v), and 0.1% digitonin (w/v), in the absence or presence of increasing concentrations of ChTX (open diamonds), sBmTX1 (open squares), or sBmTX2 (open circles). Incubations were carried out at room temperature until equilibrium was achieved (see Experimental Procedures for the conditions).

```
                1         10        20        30        40
                |         |         |         |         |
IbTX    Z-FTDVDCSVSKECWSVCKDLFGVDRG-KCMGKKCRCYQ-
ChTX    Z-FTNVSCTTSKECWSVCQRLHNTSRG-KCMNKKCRCYS-
BmTX2   Z-FTNVSCSASSQCWPVCKKLFGTYRG-KCMNSKCRCYS-
BmTX1   Z-FTDVKCTGSKQCWPVCKQMFGKPNG-KCMNGKCRCYS-
Lq2     Z-FTQESCTASNQCWSICKRLHNTNRG-KCMNKKCRCYS-

KTX     GVEINVKCSGSPQCLKPCKDA-GMRFG-KCMNRKCHCTPK
AgTX2   GVPINVSCTGSPQCIKPCKDA-GMRFG-KCMNRKCHCTPK
AgTX3   GVPINVPCTGSPQCIKPCKDA-GMRFG-KCMNRKCHCTPK
AgTX1   GVPINVKCTGSPQCLKPCKDA-GMRFG-KCINGKCHCTPK
BmKTX   -VGINVKCKHSGQCLKPCKDA-GMRFG-KCINGKCDCTPK*
KTX2    -VRIPVSCKHTGQCLKPCKDA-GMRFG-KCMNGKCDCTPK

MgTX    -TIINVKCTSPKQCLPPCKAQFGQSAGAKCMNGKCKCYPH
NTX     -TIINVKCTSPKQCSKPCKELYGSSAGAKCMNGKCKCYNN*
TsKα    -VFINAKCRGSPECLKPCKEAIGKAAG-KCMNGKCKCYP-

Pi2     -TI---SCTNPKQCYPHCKKETGYPN-AKCMNRKCKCFGR
Pi3     -TI---SCTNEKQCYPHCKKETGYPN-AKCMNRKCKCFGR
Pi1     ---L-VKCRGTSDCGRPCQQQTGCPN-SKCINRMCKCYGC
MTX     -----VSCTGSKDCYAPCRKQTGCPN-AKCINKSCKCYGC*
```

FIGURE 8: Sequence similarities between *B. martensi* toxins and some other scorpion K^+ channel inhibitors. Sequences have been aligned on the six conserved half-cystine residues. Gaps have been introduced to give maximum sequence identity. NTX, BmKTX, and MTX have an amidated C-terminal extremity denoted with an asterisk: IbTX (*13*), ChTX (*11*), Lq2 (also referred to Lqh18−2) (*12*), KTX (*14*), AgTX2,3,1 (*7*), KTX2 (*15*), MgTX (*17*), NTX (*16*), TsKα (*18*), Pi1, Pi2, and Pi3 (*9*, *10*), and MTX (*19*). Bold letters indicate amino acid residues which are highly conserved in the toxin family.

DISCUSSION

In this study, we have identified and characterized three new members of the family of K^+ channel inhibitors, from *B. martensi* scorpion venom. The complexity of *Buthidae* scorpion venoms, in terms of the number and variety of their toxins, has been demonstrated over the past years and has made the task of purification of their constituents laborious and time-consuming. Usually, investigation of crude and fractionated venom is monitored by various bioassay-guided methods. By mass fingerprinting the C18 HPLC fractions of *B. martensi* using MALDI-TOF-MS, we were able to identify several compounds with molecular masses (M_r) of 3700−4300 Da (this work) and 2900−3200 Da (*6*), which were shown to belong to the K^+ channel toxin family. As is commonly observed in other *Buthidae* venoms, and very recently in those of *Scorpionidae*, *B. martensi* venom also contained several types of K^+ channel toxins.

The three new toxins from *B. martensi* scorpion venom described in this paper display a peptidic chain of 37 amino acids and show 40−70% sequence identity with each other. Figure 8 shows their sequences aligned on the six cysteines together with some of the other K^+ channel toxins previously described. BmTX1 and BmTX2, which are 70% similar, are the most structurally related to toxins of the ChTX group, sharing with them 65−70% sequence identity, versus ca. 35% with toxins from the other three groups. BmKTX shows 81−87% sequence identity with peptides of the KTX group (henceforth referred as to BmKTX), 57−68% with

those of the NTX group, and 35−40% with those of the Pi1 group and the ChTX group. It appears that most amino acid mutations occur in variable regions (positions 20−26 in BmTX1 and BmTX2 and positions 7−12 and position 33 in BmTX1, BmTX2, and BmKTX).

The three-dimensional structure of several scorpion K^+ channel toxins has been determined by NMR spectroscopy [ChTX (*40*), IbTX (*41*), KTX (*42*, *43*), MgTX (*43*, *44*), AgTX2 (*45*), and NTX (*46*)], and the data reveal a similar fold made up of a β-sheet linked to an α-helix by disulfide bridges, supported by the consensus motif Cys-[...]-Cys-x-x-x-Cys-[...]-Cys-[...]-Cys-x-Cys. Given the presence of this motif and their high sequence similarity with previously described scorpion K^+ channel toxins, the toxins from *B. martensi*, reported in this paper, very probably adopt a similar global fold. Using the three-dimensional structure of ChTX and AgTX2 available from the Brookhaven Protein Data Bank, we have built the model of two among the Bm toxins, namely BmTX2 and BmKTX (Figure 9). Those models constitute a preliminary structural basis for discussing the impact of the mutations which distinguish BmTX2 from ChTX, and BmKTX from AgTX2, in terms of structure−activity relationships.

BmTX1 and BmTX2 are pharmacologically related to ChTX as they bind to both K_v and BK_{Ca} channels, unlike IbTX which is highly selective for BK_{Ca} channels. BmTX1 and BmTX2 were shown to interact with K_v channels, in binding competition with [^{125}I]KTX on rat brain synaptoneurosomes and in electrophysiological assays on the Kv1.3 channel expressed in *Xenopus* oocytes. They showed an affinity comparable to that of ChTX in blocking the rat Kv1.3 channel [IC_{50} of 1.5 nM for BmTX1 and 1.6 nM for BmTX2, versus 0.7 nM for ChTX (*43*)]. However, they proved to be more potent than ChTX in binding competition with [^{125}I]-KTX on rat brain synaptoneurosomes [0.09−0.17 versus 8 nM for ChTX (*23*)]. It has been demonstrated that different types of K^+ channels are present in mammalian brain, made of heterotetramers of different protein subunits [mainly Kv1.1, Kv1.2 (*29*, *38*, *39*)]. BmTX1 and BmTX2 may have a high affinity for a non-ChTX-sensitive subunit which is bound by [^{125}I]KTX.

In competition for the binding of [^{125}I]ChTX to the BK_{Ca} channels present in bovine aortic sarcolemmal membranes, BmTX1 and BmTX2 showed a lower affinity when compared to that of the unlabeled ChTX (by about 100-fold). Several hypotheses have been put forward to explain this latter modulation of activity.

Mutational analysis demonstrated that eight amino acid residues are critical for the binding of ChTX to BK_{Ca} channels [S10, W14, R25, N30, M29, R34, K27, and Y36; ChTX numbering (*21*)]. Among these eight residues, five have been described as critical for the binding of ChTX to the *Shaker* K^+ channel [K27, M29, N30, R34, and Y36 (*22*)]. These critical residues are not mutated in BmTX2, whereas the mutation R25N is found in BmTX1. This latter mutation could well be responsible for the lower affinity of BmTX1 for BK_{Ca} channels, as a similar drop in affinity was previously demonstrated for a recombinant ChTX (R25Q) (*47*). For BmTX2, the first question was whether the conserved critical residues were in a conserved position in space. This question was relevant because of the presence of a proline residue in the α-helix region of BmTX2, as well as the mutations E12Q and T9A which suppress the

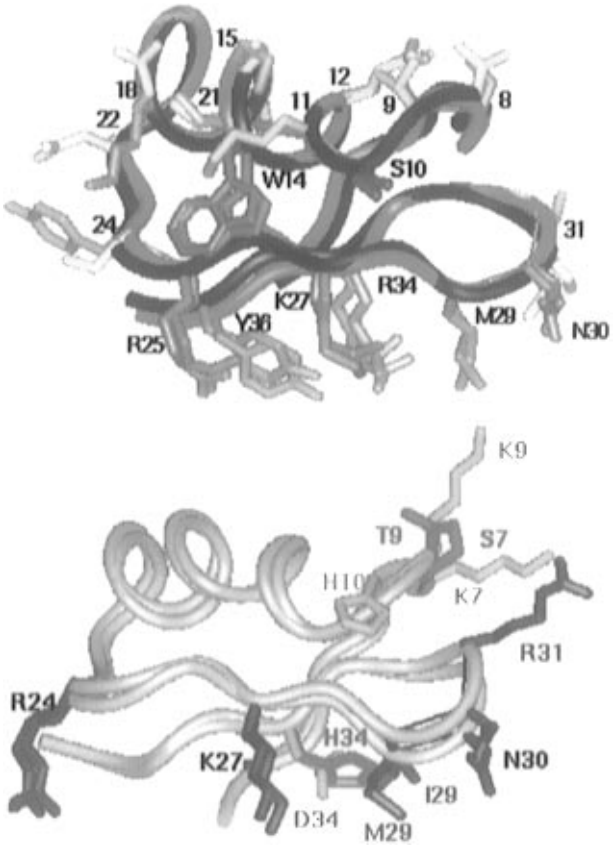

FIGURE 9: Comparison of three-dimensional structures. (Top) ChTX (*40*) and BmTX2 (modeling). Overlay of α-carbon traces (dark blue for ChTX and green for BmTX2). Selected side chains in light blue-gray illustrate the conserved residues between BmTX2 and ChTX which were shown to be critical for the binding of ChTX to BK_{Ca} channels [S10, W14, N30, M29, R34, K27, Y36, and R25 (*21*)] (the amino acid in the one-letter code and its number in the sequence are mentioned in black). Side chains of nonconserved residues are shown in yellow for ChTX or pink for BmTX2 (their number in the sequence is labeled in black). (Bottom) AgTX2 (*45*) and BmKTX (modeling). Overlay of α-carbon traces (light gray for AgTX2 and light pink for BmKTX). Numbering is based on the AgTX2 structure. Selected side chains in blue illustrate some of the critical residues in AgTX2 for interaction with the *Shaker* K^+ channel [K27, R24, N30, M29, and R31 (*52*)] which are partly conserved in BmKTX (K27, R24, and N30, in blue); mutations occur at positions 29 (Ile) and 31 (Gly). Conserved residues are labeled in black. Other mutations are indicated in yellow for BmKTX and in green for AgTX2.

N-capping interaction observed in ChTX between Glu12 and Thr9 (*48*). Comparison of our model structure of BmTX2 to the three-dimensional structure of ChTX determined by NMR (*40*) shows that the backbones of BmTX2 and ChTX are nearly identical, with subtle variations in the N- and C-terminal parts (top panel of Figure 9). We do not see any spectacular reorientation of the critical residues mentioned above (depicted in light blue in the top panel of Figure 9). In the limits of interpretation of this preliminary model structure, we conclude that the drop in affinity of BmTX2 toward BK_{Ca} channels is not due to a modulation of the orientation of the eight conserved critical residues.

Most of the mutations that distinguish BmTX2 from ChTX are clustered in a solvent-exposed surface of the α-helix (see the top panel of Figure 9, amino acids 8, 9, 11, 12, 15, 18, 21, and 22 highlighted in pink for BmTX2 and in yellow for ChTX). Two other mutations occur at positions 24 and 31 on the edges of the β-sheet and involve the residues Y24

and S31 from BmTX2 (S24 and K31 in ChTX, P24 and G31 in BmTX1). Most of those positions were tested in point mutation experiments of ChTX and showed only small effects on the binding affinity toward BK_{Ca} channels (*21*, *47*). However, one cannot exclude the possibility that those mutations, which appear at once in BmTX2 when compared to ChTX, may contribute, each at a low level, to a noticeable global effect on the affinity of the toxin.

IbTX is highly selective for BK_{Ca} channels (*13*). Attempts to achieve iodination at Y36 of IbTX led to the destruction of the biological activity of this toxin, in contrast with that of ChTX, which suffered only a slight drop in affinity (*13*). Recently, a double mutant of IbTX (IbTX-D19Y/Y36F) was engineered in order to obtain a high-specific activity radioligand for BK_{Ca} channels, iodinated on Y19 (*49*). Indeed, equilibrium binding experiments and kinetic binding analysis allowed us to determine the K_d of this double mutant of IbTX to be 5 pM, and competition studies with unlabeled IbTX and ChTX resulted in complete inhibition of binding with an affinity of about 28 and 4 pM, respectively. By contrast, IbTX was shown to be a noncompetitive inhibitor of [^{125}I]-ChTX for binding to BK_{Ca}, with an affinity of 250 pM (*13*). It will be interesting to perform saturation binding experiments to determine how BmTX1 and BmTX2 modulate the binding of [^{125}I]ChTX and [^{125}I]IbTX-D19Y/Y36F on bovine aortic smooth muscle. It is also noteworthy that BmTX2 possesses a Tyr in position 24, which does not exist in ChTX or in IbTX, and which may serve as a putative site of iodination, preferably to Y36 for reasons mentioned above.

BmKTX displays the highest percentage of sequence identity with KTX2 and AgTX1 (see Figure 8). It shows an affinity toward Kv1.3 channels of 0.6 nM for the C-carboxylated form and 0.2 nM for the C-amidated form, intermediate between that of KTX2 [0.02 nM (*50*)] and AgTX1 [1.7 nM (*7*)]. We developed a model of BmKTX, starting from the three-dimensional structure of AgTX2, determined by NMR (*45*). AgTX2 is the most potent toxin toward Kv1.3 channels [IC_{50} of 0.004 nM (*7*)]. Mutagenesis studies on AgTX2 identified a set of residues as functionally important for blocking the *Shaker* potassium channels [N30, K27, R24, S11, F25, T36, M29, and, less importantly, R31 (*51, 52*)]. Two of these residues are mutated in BmKTX, M29I and R31G (see the bottom panel of Figure 9). The R31G mutation is unlikely to drastically affect the affinity toward Kv1.3 channels, as it also occurs in KTX2. The effect of the M29I mutation could be more important; however, this mutation was previously shown to be tolerated well in ChTX for its activity toward the *Shaker* K^+ channels (*22*). Most of the other mutations are located far from the interaction surface, upstream from the α-helix (S7K, T9K, G10H, and P12G) or within the α-helix (I15L). Interestingly, the residue His34 in AgTX2, located in the *β*-sheet, is replaced by an Asp residue in BmKTX. This latter mutation could be destabilizing, as it introduces a negative charge close to the functionally important Lys27. It is noteworthy that the same mutation occurs in KTX2, but together with the mutation of Pro3 in AgTX2 into Arg3 in KTX2 (Gly3 in BmKTX), which brings a basic residue into a suitable position for forming a salt bridge with Asp34.

In conclusion, we have purified and characterized three new proteins from the venom of the Chinese scorpion *B. martensi*, which are potent inhibitors of K_v channels, two of which also interact with BK_{Ca} channels. Those new ligands should serve as useful tools for studying the structure and physiology of the K^+ channels targeted. Recently, Lq2, a toxin isolated from the venom of *L. quinquestriatus hebraeus*, was shown to be an inhibitor of the inward-rectifier K^+ channel ROMK1 (*53*); given the fact that BmTX1 and BmTX2 are closely related to Lq2, it will be interesting to test their ability to inhibit this latter channel and to assess their eventual usefulness as probes for the study of this poorly characterized K^+ channel.

ACKNOWLEDGMENT

We thank Drs. H. Minakata and A. Yasuda for their skilled advice in running the protein sequencer and performing amino acid analysis. Dr. Itagaki is acknowledged for his help with MALDI-TOF-MS.

REFERENCES

1. Garcia, M. L., Galvez, A., Garcia-Calvo, M., King, F., Vasquez, J., and Kaczorowski, G. J. (1991) *J. Bioenerg. Biomembr. 23*, 615−645.
2. Garcia, M. L., Knaus, H. G., Munujos, P., Slaughter, R. S., and Kaczorowski, G. J. (1995) *Am. J. Physiol. 38*, C1−C10.
3. Martin-Eauclaire, M. F., and Couraud, F. (1995) in *Handbook of Neurotoxicology* (Chang, L. W., and Dyer, R. S., Eds.) pp 683−716, Marcel Dekker Inc., New York.
4. Auguste, P., Hughes, M., Gravé, B., Gesquière, J. C., Maes, P., Tartar, A., Romey, G., Schweitz, H., and Lazdunski, M. (1990) *J. Biol. Chem. 265*, 4753−4759.
5. Zerrouk, H., Mansuelle, P., Benslimane, A., Rochat, H., and Martin-Eauclaire, M. F. (1993) *FEBS Lett. 320*, 189−192.
6. Romi-Lebrun, R., Martin-Eauclaire, M. F., Escoubas, P., Wu, F. Q., Lebrun, B., Hisada, M., and Nakajima, T. (1997) *Eur. J. Biochem. 245*, 457−464.
7. Garcia, M. L., Garcia-Calvo, M., Hidalgo, P., Lee, A., and MacKinnon, R. (1994) *Biochemistry 33*, 6834−6839.
8. Miller, C. (1995) *Neuron 15*, 5−10.
9. Olamendi-Portugal, T., Gómez-Lagunas, F., Gurrola, G. B., and Possani, L. D. (1996) *Biochem. J. 315*, 977−981.
10. Gomez-Lagunas, F., Olamendi-Portugal, T., Zamudio, F. Z., and Possani, L. D. (1996) *J. Membr. Biol. 152*, 49−56.
11. Gimenez-Gallego, G., Navia, M. A., Reuben, J. P., Katz, G. M., Kaczorowski, G. J., and Garcia, M. L. (1988) *Proc. Natl. Acad. Sci. U.S.A. 85*, 3329−3333.
12. Lucchesi, K., Ravindran, A., Young, H., and Moczydlowski, E. (1989) *J. Membr. Biol. 109*, 269−281.
13. Galvez, A., Gimenez-Gallego, G., Reuben, J. P., Roy-Contancin, L., Feigenbaum, P., Kaczorowski, G. J., and Garcia, M. L. (1990) *J. Biol. Chem. 265*, 11083−11090.
14. Crest, M., Jacquet, G., Gola, M., Zerrouk, H., Benslimane, A., Rochat, H., Mansuelle, P., and Martin-Eauclaire, M. F. (1992) *J. Biol. Chem. 267*, 1640−1647.
15. Laraba-Djebari, F., Legros, C., Crest, M., Ceard, B., Romi, R., Mansuelle, P., Jacquet, G., Van Rietschoten, J., Gola, M., Rochat, H., Bougis, P. E., and Martin-Eauclaire, M. F. (1994) *J. Biol. Chem. 269*, 32835−32843.
16. Possani, L. D., Martin, B. M., and Svendsen, I. B. (1982) *Carlsberg Res. Commun. 47*, 285−289.
17. Garcia-Calvo, M., Leonard, R. J., Novick, J., Stevens, S. P., Schmalhofer, W., Kaczorowski, G. J., and Garcia, M. L. (1993) *J. Biol. Chem. 268*, 18866−18874.
18. Rogowski, R. S., Krueger, B. K., Collins, J. H., and Blaustein, M. P. (1994) *Proc. Natl. Acad. Sci. U.S.A. 91*, 1475−1479.
19. Kharrat, R., Mabrouk, K., Crest, M., Darbon, H., Oughideni, R., Martin-Eauclaire, M. F., Jacquet, G., El Ayeb, M., Van Rietschoten, J., Rochat, H., and Sabatier, J. M. (1996) *Eur. J. Biochem. 242*, 491−498.
20. Ménez, A., Bontems, F., Roumestand, C., Gilquin, B., and Toma, F. (1992) *Proc. R. Soc. Edinburgh 99B*, 83−103.
21. Stampe, P., Kolmakova-Partensky, L., and Miller, C. (1994) *Biochemistry 33*, 443−450.

22. Goldstein, S. A. N., Pheasant, D. J., and Miller, C. (1994) *Neuron 12*, 1377−1388.
23. Romi, R., Crest, M., Gola, M., Sampieri, F., Jacquet, G., Zerrouk, H., Mansuelle, P., Sorokine, O., Van Dorsselaer, A., Rochat, H., Martin-Eauclaire, M.-F., and Van Rietschoten, J. (1993) *J. Biol. Chem. 268*, 26302−26309.
24. Gurrola, G. B., and Possani, L. D. (1995) *Biochem. Mol. Biol. Int. 37*, 527−535.
25. Giangiacomo, K. M., Sugg, E. E., Garcia-Calvo, M., Leonard, R. J., McManus, O. B., Kaczorowski, G. J., and Garcia, M. L. (1993) *Biochemistry 32*, 2363−2370.
26. Ji, Y. H., Hattori, H., Xu, K., and Terakawa, S. (1994) *Sci. China, Ser. B 37*, 956−963.
27. Ji, Y. H., Mansuelle, P., Terakawa, S., Kopeyan, C., Yanaihara, N., Hsu, K., and Rochat, H. (1996) *Toxicon 34*, 987−1001.
28. Romi-Lebrun, R., Lebrun, B., Escoubas, P., Pongs, O., Wu, F. Q., and Nakajima, T. (1996) *12th European Symposium on animal, plant and microbial toxins*, Basel, Switzerland, August 25−28, p 9.
29. Stühmer, W., Ruppersberg, J. P., Schröter, K. H., Sakmann, B., Stocker, M., Giese, K. P., Perschke, A., Baumann, A., and Pongs, O. (1989) *EMBO J. 8*, 3235−3244.
30. Leonard, R. J., Garcia, M. L., Slaughter, R. S., and Reuben, J. P. (1992) *Proc. Natl. Acad. Sci. U.S.A. 89*, 10094−10098.
31. Ruegg, U. T., and Rudinger, J. (1977) *Methods Enzymol. 47*, 111−116.
32. Behrens, B., and Karber, C. (1935) *Arch. Exp. Pathol. Pharmakol. 177*, 379−388.
33. Gray, E. G., and Whittaker, V. P. (1962) *J. Anat. 96*, 79−88.
34. Slaughter, R. S., Shevell, J. G., Felix, J. P., Garcia, M. L., and Kaczorowski, G. J. (1989) *Biochemistry 28*, 3995−4002.
35. Vasquez, J., Feigenbaum, P., Katz, G., King, V. F., Reuben, J. P., Roy-Contancin, L., Slaughter, R. S., Kaczorowski, G. J., and Garcia, M. L. (1989) *J. Biol. Chem. 264*, 20902−20909.
36. Meinwald, Y. C., Stimson, E. R., and Scheraga, H. A. (1986) *Int. J. Pept. Protein Res. 28*, 79−84.
37. Martin-Eauclaire, M. F., and Rochat, H. (1984) *Toxicon 22*, 695−703.
38. Scott, V. E. S., Muniz, Z. M., Sewing, S., Lichtinghagen, R., Parcej, D. N., Pongs, O., and Dolly, J. O. (1994) *Biochemistry 33*, 1617−1623.
39. Beckh, S., and Pongs, O. (1990) *EMBO J. 9*, 777−782.
40. Bontems, F., Roumestand, C., Gilquin, B., Menez, A., and Toma, F. (1991) *Science 254*, 1521−1523.
41. Johnson, B. A., and Sugg, E. E. (1992) *Biochemistry 31*, 8151−8159.
42. Fernandez, I., Romi, R., Szendeffy, S., Martin-Eauclaire, M. F., Rochat, H., Van Rietschoten, J., Pons, M., and Giralt, E. (1994) *Biochemistry 33*, 14256−14263.
43. Aiyar, J., Withka, J. M., Rizzi, J. P., Singleton, D. H., Andrews, G. C., Lin, W., Boyd, J., Hanson, D. C., Simon, M., Dethlefs, B., Lee, C. L., Hall, J. E., Gutman, G. A., and Chandy, K. G. (1995) *Neuron 15*, 1169−1181.
44. Johnson, B. A., Stevens, S. P., and Williamson, J. M. (1994) *Biochemistry 33*, 15061−15070.
45. Krezel, A. M., Kasibhatla, C., Hidalgo, P., MacKinnon, R., and Wagner, G. (1995) *Protein Sci. 4*, 1478−1489.
46. Dauplais, M., Gilquin, B., Possani, L. D., Gurrola-Briones, G., Roumestand, C., and Menez, A. (1995) *Biochemistry 34*, 16563−16573.
47. Park, C. S., and Miller, C. (1992) *Biochemistry 31*, 7749−7755.
48. Dyke, T. R., Duggan, B. M., Pennington, M. W., Byrnes, M. E., Kem, W. R., and Norton, R. S. (1996) *Biochim. Biophys. Acta 1292*, 31−38.
49. Koschak, A., Koch, R. O., Liu, J., Kaczorowski, G. J., Reinhart, P. H., Garcia, M. L., and Knaus, H.-G. (1997) *Biochemistry 36*, 1943−1952.
50. Fremont, V., Crest, M., Romi, R., Rochat, H., Martin-Eauclaire, M.-F., Gola, M., and Van Rietschoten, J. (1996) *24th Symposium of the European Peptide Society*, Edinburgh, Scotland, September 8−13.
51. Hidalgo, P., and MacKinnon, R. (1995) *Science 268*, 307−310.
52. Ranganathan, R., Lewis, J. H., and MacKinnon, R. (1996) *Neuron 16*, 131−139.
53. Lu, Z., and MacKinnon, R. (1997) *Biochemistry 36*, 6936−6940.

BI971044W